

This is the accepted manuscript made available via CHORUS. The article has been published as:

# Local sublattice-symmetry breaking in rotationally faulted multilayer graphene

M. Kindermann and P. N. First

Phys. Rev. B **83**, 045425 — Published 31 January 2011

DOI: [10.1103/PhysRevB.83.045425](https://doi.org/10.1103/PhysRevB.83.045425)

# Local sublattice-symmetry breaking in rotationally faulted multilayer graphene

M. Kindermann and P. N. First

*School of Physics, Georgia Institute of Technology, Atlanta, Georgia 30332, USA*

(Dated: December 9, 2010)

Interlayer coupling in rotationally faulted graphene multilayers breaks the local sublattice-symmetry of the individual layers. We present a theory of this mechanism, which reduces to an effective Dirac model with space-dependent mass in an important limit. It thus makes a wealth of existing knowledge available for the study of rotationally faulted graphene multilayers. We demonstrate quantitative agreement between our theory and a recent experiment.

PACS numbers: 73.20.-r, 73.21.Cd, 73.22.Pr

## INTRODUCTION

Experiments indicate that the 10–100 individual graphene layers grown on the carbon-terminated face of SiC are surprisingly well decoupled from one another electronically. Early spectroscopic measurements [1, 2] found a linear low-energy electronic dispersion to the experimental precision, like that of single-layer graphene [3, 4]. In scanning tunneling microscopy/spectroscopy (STM/STS) measurements the Landau level quantization of the material in a magnetic field was found to be essentially that of single-layer graphene [5]. Theoretically it has been shown that this approximate decoupling of different layers is due to a relative twist of the layers with respect to each other [6–12]. A renormalization of the electron velocity [7, 11], van Hove singularities [13], and interlayer transport [14] have been discussed as residual effects of the interlayer coupling.

In a recent STM measurement on multilayer epitaxial graphene [15] a spatially modulated splitting  $\Delta \lesssim 10$  meV of the zeroth Landau level ( $LL_0$ ) was observed. In view of the above this finding is intriguing, since the states forming  $LL_0$  of an isolated layer of graphene without electron-electron interactions are degenerate. Therefore, either the observed splitting of  $LL_0$  is due to electron-electron interactions, or the interlayer coupling manifests itself prominently in this measurement. In many ways the experimental data favors the latter scenario. One such indication is the observation of a sublattice polarization of the split  $LL_0$ : there are regions of space where the branch of  $LL_0$  that has positive energy  $\Delta/2$  appears to consist of wavefunctions localized on the A-sublattice of the graphene lattice, while the lower branch, at negative energy  $-\Delta/2$ , is localized on the B-sublattice. The implied local sublattice-symmetry breaking has a natural explanation in terms of the interlayer coupling: the coupling to lower graphene layers generically induces a difference between the local environments of the two sublattices of the top layer in the material, which is probed in STM. This is illustrated in Fig. 1 for a stack of two graphene layers with a relative twist. There are regions where atoms on the A-sublattice of the top layer are closer to atoms in the bottom layer

than those on the B-sublattice of the top layer and regions with the reverse situation. A second conspicuous feature of the STM data is a spatial modulation of the splitting of  $LL_0$ : the regions where  $LL_0$  is split appear to be arranged on a hexagonal superlattice with a lattice constant  $l \approx 70$  nm. It thus shares the symmetries of the moiré pattern characteristic of the twisted graphene bilayer shown in Fig. 1—another strong indication that the observed splitting is due to the interlayer coupling.

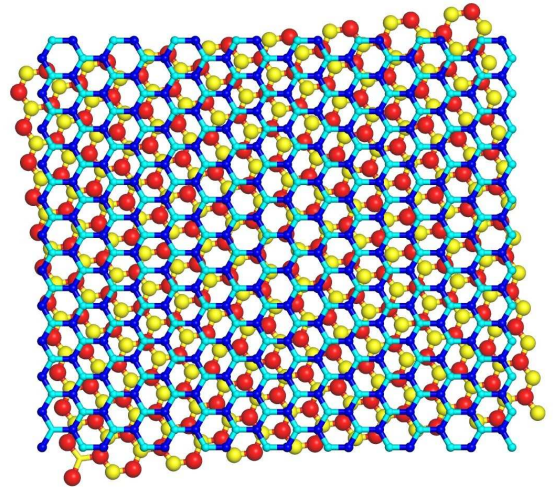


FIG. 1: (color online) Moiré pattern created by two graphene lattices with a relative twist. Top layer A/B sublattice atoms are shown as small blue/cyan (dark/light) spheres and connectors; bottom layer A/B atoms are shown as large red/yellow (dark/light) spheres. A region of AA alignment lies at the center, where each top-layer atom has a neighbor in the bottom layer. The AA region is surrounded by three AB- and three BA-aligned regions where atoms on only one top-layer sublattice have direct neighbors in the bottom layer. As a consequence, the sublattice-symmetry is broken locally.

Earlier theory of the interlayer coupling in graphene multilayers did not predict the observed splitting of  $LL_0$ . In Ref. [15] we therefore proposed a phenomenological theory, modeling the different local environments of the A- and the B-atoms of the top graphene layer by a “staggered” electric potential  $V_{AB}$  that has opposite sign on the two sublattices. This model qualitatively accounts for

the main features of the experimental data. In this article we present a microscopic theory of the interlayer coupling in rotationally faulted graphene multilayers. We reduce the problem to an effective model of the top layer of the material, which is probed in many experiments, such as STM. In order to conveniently explain the rich spatial structure of the system illustrated in Fig. 1 and observed in Ref. [15] we formulate our theory in real space, as distinct from prior momentum-space approaches [7, 11, 14]. The resulting Hamiltonian reduces to the phenomenological model of Ref. [15] in certain limits and it likewise reproduces the main qualitative features of the measurements. Our theory moreover allows us to test quantitatively whether the interlayer coupling can explain the experimental findings [15]. The answer is affirmative: using the commonly accepted tight-binding parameters of graphene multilayers our theory predicts both the magnitude of the observed splitting and its magnetic field dependence in very good agreement with experiment.

## MODEL

We analyze the electron dynamics in a graphene layer “0” when coupled to a second layer “1,” twisted by a relative angle  $\theta$  ( $\theta = 0^\circ$  for aligned honeycomb lattices, *cf.* Fig. 1), neglecting electron-electron interactions. The corresponding dynamics in multilayers at perturbatively weak interlayer coupling, such as in the experiment [15], are obtained by summation over all layers coupled to the top layer 0. Twisted graphene bilayers have been described before [7, 9–12] by a local interlayer coupling Hamiltonian with parameters fitted to experiment [16],

$$H_{\text{int}} = \int d\mathbf{r} \Psi^{(0)\dagger}(\mathbf{r}) \Gamma(\mathbf{r}) \Psi^{(1)}(\mathbf{r}) + h.c. \quad (1)$$

Here, the spinors  $\Psi^{(j)}$  collect the amplitudes for electrons on the two sublattices of layer  $j \in \{0, 1\}$ . The interlayer coupling  $\Gamma$  has contributions at wavevectors  $\mathbf{b}^{(0)} - \mathbf{b}^{(1)}$ , where  $\mathbf{b}^{(j)}$  are reciprocal vectors of the graphene lattice in layer  $j$  [12]. The Fourier components of  $\Gamma$  quickly decay with increasing wavevector [9, 10, 12]. In this article we therefore neglect all but the zero wavevector component, setting  $\Gamma(\mathbf{r}) = \gamma$ . In the “first star approximation” of the wavefunctions employed below, the distinction between commensurate and incommensurate interlayer rotations then disappears. This approximation is valid for energies  $\varepsilon \gg \mathcal{V}$ , where  $\mathcal{V}$  is set by the Fourier components of  $\Gamma$  that directly connect K-points of the two layers [12]. We take the limit  $0 < \theta \ll 1$ , when  $\mathcal{V} \ll \gamma$  (in the experiment [15]  $\theta \approx 0.25^\circ$  and according to the estimate  $\mathcal{V} \simeq \theta^2 \gamma$  of Ref. [12] this approximation is justified at all accessed energies).

In our limit  $0 < \theta \ll 1$  a long-wavelength description is appropriate, where the isolated layers  $j$  are described

by Dirac model Hamiltonians (we set  $\hbar = 1$ )

$$H^{(j)} = v \int d\mathbf{r} \sum_{\nu} \psi_{\nu}^{(j)\dagger}(\mathbf{r}) [\boldsymbol{\sigma}_{\nu} \cdot (-i\nabla + e\mathbf{A}(\mathbf{r}))] \psi_{\nu}^{(j)}(\mathbf{r}). \quad (2)$$

Here,  $\boldsymbol{\sigma}_{\nu} = (\nu\sigma_x, \sigma_y)$  is a vector of Pauli matrices,  $\nu = \pm$  is the valley spin,  $-e$  the electron charge, and  $v$  the electron velocity in graphene. We have included an external vector potential  $\mathbf{A}$  to describe a perpendicular magnetic field  $B$ . Eq. (2) acts on the long-wavelength spinors  $\psi_{\mu\nu}^{(j)}$  defined by  $\Psi_{\mu}^{(j)}(\mathbf{r}) = \sum_{\nu} u_{\mu\nu}^{(j)}(\mathbf{r}) \psi_{\mu\nu}^{(j)}(\mathbf{r})$ . We write the Bloch functions  $u_{\mu\nu}^{(j)}(\mathbf{r}) = \{\sum_p \exp[i\mathbf{K}_{p\nu}^{(j)} \cdot (\mathbf{r} - \boldsymbol{\tau}_{\mu}^{(j)})]\} / \sqrt{3}$  in the “first star approximation” appropriate for the interlayer coupling problem [12]. Here,  $p$  sums over the three equivalent Brillouin zone corners  $\mathbf{K}_{p\nu}^{(j)}$  that form the Dirac point of valley  $\nu$  [12] and  $\boldsymbol{\tau}_{\mu}^{(j)}$  gives the position of an atom on sublattice  $\mu \in \{A, B\}$  within the unit cell of layer  $j$ . In the long-wavelength theory (which neglects inter-valley processes) the interlayer coupling reads

$$H_{\text{int}} = \int d\mathbf{r} \sum_{\nu} \psi_{\nu}^{(0)\dagger}(\mathbf{r}) t_{\nu}(\mathbf{r}) \psi_{\nu}^{(1)}(\mathbf{r}) + h.c., \quad (3)$$

with a matrix  $t$  whose long-wavelength components have wavevectors  $\delta\mathbf{K}_{p\nu} = (R_{\theta} - 1)\mathbf{K}_{p\nu}^{(0)}$ . Here,  $R_{\theta}$  is a rotation around the  $z$ -axis by angle  $\theta$ . Retaining only those long-wavelength parts of  $t$  we find

$$t_{\nu}^{\mu\mu'}(\mathbf{r}) = \frac{\gamma}{3} \sum_p e^{i\delta\mathbf{K}_{p\nu} \cdot \mathbf{r} + i\mathbf{K}_{p\nu} \cdot (\boldsymbol{\tau}_{\mu}^{(0)} - \boldsymbol{\tau}_{\mu'}^{(1)})}, \quad (4)$$

where terms of order  $\theta$  are neglected, while terms of order  $\theta Kr$  are kept as they may grow large.

## EFFECTIVE THEORY

We next integrate out layer  $j = 1$  in order to arrive at an effective Hamiltonian  $H_0^{\text{eff}}(\omega) = H_0 + \delta H_0^{\text{eff}}(\omega)$  for the top layer  $j = 0$ , with

$$\delta H_0^{\text{eff}}(\omega) = H_{\text{int}}(\omega + V - H_1)^{-1} H_{\text{int}}. \quad (5)$$

We include an interlayer bias  $V$  that accounts for different doping levels of the two layers [24]. In general,  $H_0^{\text{eff}}$  is nonlocal in space and it depends on the energy  $\omega$ . In the limit of a large interlayer bias, however,  $|V| \gg \omega, \gamma, \theta v/a$ , the sum  $\omega + V - H_1$  becomes momentum- and energy-independent to a good approximation. The spatial nonlocality and the energy-dependence of  $H_0^{\text{eff}}$  then may be neglected and  $H_0^{\text{eff}}$  becomes a conventional Dirac Hamiltonian (2) with a matrix potential

$$\delta H_0^{\text{eff}} = \int d\mathbf{r} \sum_{\nu} \psi_{\nu}^{(0)\dagger}(\mathbf{r}) \frac{t_{\nu}(\mathbf{r}) t_{\nu}^{\dagger}(\mathbf{r})}{V} \psi_{\nu}^{(0)}(\mathbf{r}), \quad (6)$$

which we parametrize as

$$\frac{t_\nu(\mathbf{r})t_\nu^\dagger(\mathbf{r})}{V} = V^{\text{eff}}(\mathbf{r}) + \nu v e \boldsymbol{\sigma}_\nu \cdot \mathbf{A}^{\text{eff}}(\mathbf{r}) + m^{\text{eff}}(\mathbf{r})v^2\sigma_z. \quad (7)$$

The interlayer coupling in this limit generates effective scalar and vector potentials  $V^{\text{eff}}$  and  $\mathbf{A}^{\text{eff}}$ , respectively, and a mass term  $\propto \sigma_z m^{\text{eff}} v^2$  that implies an effective staggered potential  $V_{AB}^{\text{eff}} = m^{\text{eff}} v^2$  in locally Bernal stacked regions. It follows from Eq. (4) that  $\delta H_{0\nu}^{\text{eff}}$  oscillates in space with wavevectors  $\mathbf{k} = (R_\theta - 1)\mathbf{b}$ , where  $\mathbf{b}$  is in the “first star” of reciprocal lattice vectors of graphene. We plot  $\delta H_{0\nu}^{\text{eff}}$  in the parameterization of Eq. (7) in Fig. 2.

## COMPARISON WITH EXPERIMENT

Now turning to the experiment [15] we note that at large interlayer bias  $V$  our theory takes the form of the phenomenological Hamiltonian proposed in Ref. [15]. It then intuitively explains the main qualitative features of the experiment: perturbatively in  $\gamma$ , the energy shift of a  $\text{LL}_0$  wavefunction  $\psi_{0\nu}$  in valley  $\nu$  is given by

$$\delta \varepsilon_{0\nu} = \langle \psi_{0\nu} | \delta H_{0\nu}^{\text{eff}}(\omega = 0) | \psi_{0\nu} \rangle. \quad (8)$$

The unperturbed  $\text{LL}_0$  wavefunctions are localized on individual sublattices. Therefore, if  $\delta H_{0\nu}^{\text{eff}}$  included a constant staggered potential  $V_{AB} > 0$ , with potentials  $V_{AB}$  and  $-V_{AB}$  for atoms on the A- and B-sublattice, respectively, a splitting  $\Delta = \delta \varepsilon_{0,\nu=1} - \delta \varepsilon_{0,\nu=-1} = -2V_{AB}$  between sublattice-polarized  $\text{LL}_0$  states would result, as observed experimentally:  $V_{AB}$  would increase the energy of the states  $\psi_{0,\nu=-1}$  localized on the A-sublattice and decrease the energy of the  $\nu = 1$  states, localized on the B-sublattice. For the space-dependent  $V_{AB}^{\text{eff}} = m^{\text{eff}} v^2$  of Fig. 2 that splitting is still present locally, around the extrema of  $m^{\text{eff}}$ , at sufficiently large magnetic fields  $B$ , when the  $\text{LL}_0$  wavefunctions fit well into the regions with extremal  $m^{\text{eff}}$ . Comparison of Fig. 2 with Fig. 5a of Ref. [15] shows that the thus predicted spatial symmetries of  $|\Delta| \propto |m^{\text{eff}}|$  agree with experiment. For large  $B$  the splitting approaches  $\lim_{B \rightarrow \infty} \Delta = -2V_{AB}^{\text{eff}}$ . With decreasing  $B$ , as the wavefunctions become more extended,  $\Delta$  gets averaged over maxima and minima of  $m^{\text{eff}}$  and it is suppressed, also in accordance with experiment.

The experiment of Ref. [15], however, was not done in the high bias limit. The fact that in the measurement [15] tunneling into  $\text{LL}_0$  occurred only at a finite bias voltage  $V_{\text{STM}} \approx 60$  meV between STM-tip and sample does indicate a doping of the graphene layers at the surface. The difference between the chemical potentials of the top layer and the layers below after screening is expected to be  $|V| \lesssim V_{\text{STM}} \approx 60$  meV. However, the large applied magnetic field  $4 \text{ T} \leq B \leq 8 \text{ T}$  corresponds to a large cyclotron frequency  $\omega_c = \sqrt{2}v/l_B$  [17], where  $l_B = 1/\sqrt{eB}$

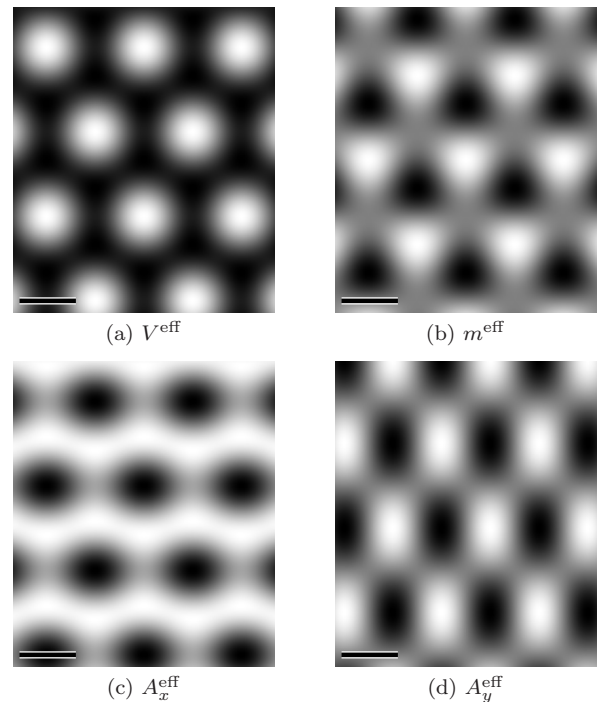


FIG. 2: (a) Effective potential  $V^{\text{eff}}$ , (b) effective mass  $m^{\text{eff}}$ , (c)  $A_x^{\text{eff}}$ , and (d)  $A_y^{\text{eff}}$  of Eq. (7) as functions of  $\mathbf{r}\theta/a$  in grey-scale. Scale bars span a unity increment in  $\mathbf{r}\theta/a$ . Note the expected sixfold and threefold symmetries of  $V^{\text{eff}}$  and  $m^{\text{eff}}$ , respectively.  $\mathbf{A}^{\text{eff}}$  transforms as a vector under rotations.

is the magnetic length:  $\omega_c \approx 105$  meV at  $B = 8$  T. In this experiment therefore  $|V| < \omega_c$  and  $H_0^{\text{eff}}$  is not local on the scale  $l_B$  on which the wavefunctions vary.

The experiment also indicates that it is the coupling between the top layer and its next-to-nearest layer (that is the third layer from the top) that produces the observed splitting. One concludes this from the observation that the dominant moiré of the STM topography, most likely due to the coupling of the top layer to its nearest neighbor, has a much smaller lattice constant  $\bar{l} \approx 4$  nm than the superlattice associated with the splitting of  $\text{LL}_0$  with  $l \approx 70$  nm. The estimates of the next-to-nearest layer coupling in the literature vary [16, 18–20], but there is a consensus that the coupling constant is  $\gamma \lesssim 40$  meV. The physics at the energies  $\omega = \pm\Delta/2 \approx \pm 5$  meV where the splitting of  $\text{LL}_0$  occurs is thus described by  $H_0^{\text{eff}}$  at  $|\omega|, \gamma \ll |V| \ll \omega_c$ . In this limit the effects of the interlayer coupling are perturbative, which allows us to deal with the non-locality of  $H_0^{\text{eff}}$  analytically. We evaluate Eq. (8) at  $|\omega|, \gamma \ll |V| \ll \omega_c$  in the appendix. In accordance with the intuition gained from the limit  $V \rightarrow \infty$  of the previous paragraph, the resulting  $\Delta$  is extremal in locally Bernal stacked regions and the wavefunctions are sublattice-polarized. The qualitative agreement with experiment thus carries over to the non-local theory.

Now comparing our theory also quantitatively with the



experiment we first take the limit of a large magnetic field, when the wavefunctions fit well into the Bernal stacked regions. The maximal splitting  $\Delta_{\max}$ , reached at  $B \rightarrow \infty$  in AB- or BA-stacked regions, can be extracted from Eq. (20) of the appendix by taking the limit  $\theta \rightarrow 0$  at fixed  $B$ . We find

$$|\Delta_{\max}| = |V| \left| \frac{\gamma}{\omega_c} \right|^2 \quad (9)$$

in our approximations. Estimating  $\gamma$  by  $\gamma = \gamma_5 \approx 38 \text{ meV}$  given in Ref. [19] we find that  $|\Delta_{\max}| \approx 5 \text{ meV}$  for  $V \approx 40 \text{ meV}$ . Considering the uncertainties in our knowledge of  $\gamma$  and  $V$ , this agrees well with the experimentally observed value  $\Delta \approx 10 \text{ meV}$ .

We next quantify the magnetic field dependence of  $\Delta$  in the regions with maximal  $\Delta$  at  $B \rightarrow \infty$  (that is AB- or BA-stacked regions) by expanding Eq. (20) asymptotically for  $\delta K l_B \gg 1$ :

$$|\Delta| \sim \frac{2|V|}{\sqrt{3}} \left| \frac{\gamma}{v \delta K} \right|^2 e^{-B_*/B} \times \left| \cos \left( \frac{\sqrt{3} B_*}{5B} - \frac{\pi}{6} \right) - \frac{2v \delta K}{V} \cos \left( \frac{\sqrt{3} B_*}{5B} + \frac{\pi}{6} \right) \right|. \quad (10)$$

The crossover field  $B_* = 5(\delta K)^2/4e$ , where the exponent in Eq. (10) becomes of order 1 and  $\Delta$  starts to be exponentially suppressed, evaluates to  $B_* = 4.8 \text{ T}$  for the interlayer rotation angle  $\theta = 0.25^\circ$  of the moiré pattern in the experiment of Ref. [15]. Also that crossover field compares favorably with the experiment, where the splitting  $\Delta$  disappears between  $B \approx 4 \text{ T}$  and  $B \approx 6 \text{ T}$ . Clearly therefore, the interlayer coupling can account for the main features of the splitting of  $\text{LL}_0$  reported in Ref. [15] also on a quantitative level.

We finally discuss the influence of the graphene layers in the experimental sample that we have ignored so far. The coupling of the top layer to layers further away than the third layer from the top is negligibly small. The coupling  $\bar{\gamma}$  to the second layer, however, is not:  $\bar{\gamma} \approx 0.4 \text{ eV}$  [18]. As mentioned before, the STM topography of Ref. [15] has a moiré pattern with scale  $\bar{l} \approx 4 \text{ nm}$ , which indicates a rotation angle between the top two layers of  $\bar{\theta} \approx 4^\circ$ . At this angle the coupling between the “first stars” of the Brillouin zones of those two layers is perturbative, because of large energy denominators [7]. The coupling between other  $K$ -points in the extended Brillouin zone is too small to play a role at the scale of the observed splitting  $\Delta$  [12]. The perturbative calculation outlined in the appendix therefore describes also the coupling between the top two layers of the measured sample. Applying Eq. (10) to that coupling we find an exponential suppression of  $\Delta$  that is lifted only above a crossover field  $\bar{B}_* = (\bar{\theta}/\theta)^2 B_* \approx 300 B_*$  that is much larger than the experimentally applied fields. The only interlayer coupling relevant to the experiment of Ref. [15] is therefore the next-to-nearest layer coupling discussed above.

## CONCLUSIONS

We conclude that the interlayer coupling is a viable explanation of the splitting of  $\text{LL}_0$  reported in Ref. [15], both qualitatively and quantitatively. The theory that allowed us to reach these conclusions reduces in certain limits to an effective Dirac model for the top layer of a multilayer system, with effective potentials and a space-dependent mass. As such it makes the wealth of knowledge and intuition existing for the physics of single layer graphene available for the study of rotationally faulted multilayer graphene. Our theory thus appears to be an advantageous starting point for the exploration of much of the physics of this rather complex system. Numerous unconventional and so far unexplained phenomena observed in the material [21] as well as known properties of our theory promise that such exploration will be rewarding. Especially the effective mass term is expected to have profound implications, for instance topologically confined states [22, 23].

We gratefully acknowledge discussions with E. J. Mele, D. L. Miller, P. San-Jose, and A. Lamacraft. This work was funded in part by the NSF (DMR-0804908) and by the Semiconductor Research Corporation Nanoelectronics Research Initiative (NRI-INDEX).

## Appendix: Perturbative Landau level splitting in a large magnetic field

We evaluate the splitting  $\Delta = \delta \varepsilon_{0,\nu=1} - \delta \varepsilon_{0,\nu=-1}$  between the two valleys of  $\text{LL}_0$  at  $|\omega|, \gamma \ll |V| \ll \omega_c$ , when it is perturbative, using Eq. (8) with localized wavefunctions of  $\text{LL}_0$ :  $\psi_{0,\nu=1} = (0, \exp[-(x^2 + y^2)/4l_B^2 + ixy/2l_B^2]/\sqrt{2\pi}l_B)$  and  $\psi_{0,\nu=-1} = \sigma_y \psi_{0,\nu=1}$ . We write the effective Hamiltonian as

$$\delta H_\nu^{\text{eff}}(\mathbf{r}, \mathbf{r}', \omega) = t_\nu(\mathbf{r}) G_\nu(\omega, \mathbf{r}, \mathbf{r}') t_\nu^\dagger(\mathbf{r}'), \quad (11)$$

where

$$G_\nu(\omega, \mathbf{r}, \mathbf{r}') = \int \frac{dk}{2\pi} \sum_{n \geq 0, s=\pm} \frac{\psi_{snk\nu}(\mathbf{r}) \psi_{snk\nu}^\dagger(\mathbf{r}')}{\omega + V - s\varepsilon_n} \quad (12)$$

with

$$\psi_{snk,\nu=1}(\mathbf{r}) = \frac{1}{\sqrt{2}l_B} \begin{pmatrix} \Phi_{n-1} \left( \frac{y}{l_B} - kl_B \right) \\ s\Phi_n \left( \frac{y}{l_B} - kl_B \right) \end{pmatrix} e^{ikx} \quad (n \geq 0) \quad (13)$$

in terms of the oscillator wavefunctions

$$\Phi_n(\chi) = \frac{(-1)^n}{\sqrt{2^n n!} \sqrt{\pi}} e^{\chi^2/2} \frac{d^n}{d\chi^n} e^{-\chi^2}. \quad (14)$$

Here,  $\Phi_{-1} = 0$ ,  $\varepsilon_n = \sqrt{n}\omega_c$  and the wavefunctions in the valley  $\nu = -1$  are obtained as  $\psi_{snk,\nu=-1} = \sigma_y \psi_{snk,\nu=1}$ .

In our limit  $|V| \ll \omega_c$ , the contribution to  $\delta\varepsilon_{0\nu}$  with the smallest energy denominator comes from the term in Eq. (12) with  $n = 0$ . That term is  $\propto |t_{BB}|^2$  in valley  $\nu = 1$ . In valley  $\nu = -1$  the corresponding term is identical, except that  $t_{BB}$  is replaced by  $t_{AA}$ . One has  $t_{BB} = t_{AA} + \mathcal{O}(\theta)$  [25]. To leading order in  $\theta$  this term therefore does not contribute to  $\Delta$ . The dominant contribution to  $\delta\varepsilon_0$  thus comes from the off-diagonal elements of  $\delta H^{\text{eff}}$  and from the diagonal elements that are  $\propto |t_{AB}|^2$  or  $\propto |t_{BA}|^2$  [the upper diagonal element in Eq. (12) at  $\nu = 1$ ]. In those matrix elements all contributing energy denominators are of the same order,  $\mathcal{O}(\omega_c)$ . We thus need to carry out the sum over  $n$  in Eq. (12). We do this below for  $G_1$ . The Green function in the other valley is then obtained as  $G_{-1} = \sigma_y G_1 \sigma_y$ . We first rewrite Eqs. (12) with (13) and (14) as

$$G_1(\omega, \mathbf{r}, \mathbf{r}') = \int \frac{dk}{2\pi} e^{ik(x-x') + [(y/l_B - kl_B)^2 + (y'/l_B - kl_B)^2]/2} \times g\left(\omega, \frac{y}{l_B} - kl_B, \frac{y'}{l_B} - kl_B\right) \quad (15)$$

and note that in our limit  $|\omega| \ll |V| \ll \omega_c$  the component  $g_{AA}$ , which makes one of the leading contributions to  $\Delta$  according to the above considerations, can be expressed as

$$g_{AA}(0, \chi, \chi') = \frac{\sqrt{\pi}V}{2\omega_c^2} l(\chi, \chi') + \mathcal{O}\left(\frac{V^2}{\omega_c^3}\right) \quad (16)$$

in terms of a function  $l$  that solves the differential equation

$$\frac{\partial^2 l}{\partial \chi \partial \chi'} = -\frac{4}{\sqrt{\pi}} \sum_{n \geq 1} \Phi_n(\chi) \Phi_n(\chi') e^{-(\chi^2 + \chi'^2)/2}. \quad (17)$$

Using the completeness of the oscillator wavefunctions we find that Eq. (17) is solved by

$$l(\chi, \chi') = [\text{erf}(\chi) - \text{sgn}(\chi - \chi')] [\text{erf}(\chi') + \text{sgn}(\chi - \chi')] + f(\chi) + f'(\chi') \quad (18)$$

with arbitrary functions  $f$  and  $f'$ . Exploiting the symmetries  $g(\omega, \chi', \chi) = g(\omega, \chi, \chi')$  and  $g(\omega, -\chi, -\chi') = g(\omega, \chi, \chi')$  that are implied by Eqs. (12) and (15), one finds that  $f = f'$  and that  $f$  is an odd function of  $\chi$ . Now noting that according to Eq. (12)  $\langle \Phi_n | G(\omega) | \Phi_m \rangle = 0$  for  $n \neq m$  one concludes that  $f = 0$  [26]. The off-diagonal matrix elements of  $g$  are found similarly. To leading order in  $V$  they read

$$g_{AB}(0, \chi, \chi') = \frac{\sqrt{2\pi}}{4\omega_c} \frac{\partial}{\partial \chi'} l(\chi, \chi') + \mathcal{O}\left(\frac{V}{\omega_c^2}\right), \\ g_{BA}(0, \chi, \chi') = g_{AB}(0, \chi', \chi). \quad (19)$$

Eqs. (11), (15), (16), (18), and (19) allow us to evaluate  $\delta\varepsilon_{0,\nu=1}$ , Eq. (8), to leading order in  $\gamma$ , yielding

$$\delta\varepsilon_{0,\nu=1} = \frac{V}{2\omega_c^2} \int d\chi d\chi' \sum_{p,p'} [\text{erf}(\chi) - \text{sgn}(\chi - \chi')] [\text{erf}(\chi') + \text{sgn}(\chi - \chi')] \\ \times \left\{ t_{BA}^*(\delta\mathbf{K}_p) t_{BA}(\delta\mathbf{K}_{p'}) + (\omega_c/\sqrt{2}V) [t_{BB}^*(\delta\mathbf{K}_p) t_{BA}(\delta\mathbf{K}_{p'}) (\mathbf{c} \cdot \delta\mathbf{K}_{p'})^* + t_{BA}^*(\delta\mathbf{K}_p) t_{BB}(\delta\mathbf{K}_{p'}) (\mathbf{c} \cdot \delta\mathbf{K}_p)] \right\} \\ \times e^{-l_B^2 [(2(\delta\mathbf{K}_{p,x} - \delta\mathbf{K}_{p',x})^2 + (\delta\mathbf{K}_{p,x} + \delta\mathbf{K}_{p',x})^2 + (\delta\mathbf{K}_{p,y} - \delta\mathbf{K}_{p',y})^2 + 2i(\delta\mathbf{K}_{p,x} + \delta\mathbf{K}_{p',x})(\delta\mathbf{K}_{p,y} - \delta\mathbf{K}_{p',y}))]/4 - l_B[(\mathbf{c} \cdot \delta\mathbf{K}_p)\chi + (\mathbf{c} \cdot \delta\mathbf{K}_{p'})^* \chi']}, \quad (20)$$

where scalar multiplication with  $\mathbf{c} = (1, i)$  maps a vector  $\mathbf{a}$  onto its counterpart  $\mathbf{c} \cdot \mathbf{a}$  in the complex plane. Here, all wavevectors  $\delta\mathbf{K}_p$  are evaluated in valley  $\nu = 1$ . The energy shift  $\delta\varepsilon_{0,\nu=-1}$  in the other valley is obtained as in Eq. (20), but with  $t$  replaced by  $\sigma_y t \sigma_y$  and  $\delta\mathbf{K}_p$  evaluated in valley  $\nu = -1$ . In Eq. (9) of the main text, that is in the limit of large  $B$ , only the first term in the curly brackets of Eq. (20) contributes and the resulting splitting  $\Delta$  has extrema in regions where the layers are

locally Bernal stacked and  $|t_{BA}|^2 - |t_{AB}|^2$  is extremal.

In the limit  $B \rightarrow 0$ , when the wavefunctions become more and more extended and start averaging over several unit cells of the moiré superlattice, the splitting of  $\text{LL}_0$  decays to zero. In order to quantify this decay of  $\Delta$ , Eq. (20) may be expanded asymptotically in a large  $\delta K l_B$ . Then  $\delta\varepsilon_{0\nu}$  is dominated by the terms with the weakest exponential decay in  $\delta K l_B$ , which give

$$\begin{aligned}
\delta\varepsilon_{0,\nu=1} \sim & V \sum_{p,p'} \frac{t_{\text{BA}}^*(\delta\mathbf{K}_p)t_{\text{BA}}(\delta\mathbf{K}_{p'}) + (\omega_c/\sqrt{2}V) [t_{\text{BB}}^*(\delta\mathbf{K}_p)t_{\text{BA}}(\delta\mathbf{K}_{p'}) (\mathbf{c} \cdot \delta\mathbf{K}_{p'})^* + t_{\text{BA}}^*(\delta\mathbf{K}_p)t_{\text{BB}}(\delta\mathbf{K}_{p'}) (\mathbf{c} \cdot \delta\mathbf{K}_p)]}{v^2 (\mathbf{c} \cdot \delta\mathbf{K}_p) (\mathbf{c} \cdot \delta\mathbf{K}_{p'})^*} \\
& \times e^{-l_B^2 [(\delta\mathbf{K}_p - \delta\mathbf{K}_{p'})^2 + \delta\mathbf{K}_p \cdot \delta\mathbf{K}_{p'} - i(\delta\mathbf{K}_p \times \delta\mathbf{K}_{p'}) \cdot \hat{z}]/2}
\end{aligned} \tag{21}$$


---

at  $\delta K l_B \gg 1$ . Here,  $\hat{z}$  is the unit vector along the  $z$ -axis. Again all wavevectors  $\delta\mathbf{K}_p$  are evaluated in valley  $\nu = 1$  and  $\delta\varepsilon_{0,\nu=-1}$  in the other valley is obtained by replacing  $t$  with  $\sigma_y t \sigma_y$  in Eq. (21) and evaluating  $\delta\mathbf{K}_p$  in valley  $\nu = -1$ . The sum over  $p$  and  $p'$  in Eq. (21) results in Eq. (10) of the main text.

- 
- [1] M. L. Sadowski, G. Martinez, M. Potemski, C. Berger, and W. A. de Heer, Phys. Rev. Lett. **97**, 266405 (2006).
- [2] M. Orlita, C. Faugeras, P. Plochocka, P. Neugebauer, G. Martinez, D. K. Maude, A.-L. Barra, M. Sprinkle, C. Berger, W. A. de Heer, M. Potemski, Phys. Rev. Lett. **101**, 267601 (2008).
- [3] K. Novoselov, A. Geim, S. Morozov, D. Jiang, Y. Zhang, S. Dubonos, I. Grigorieva, and A. Firsov, Science **306**, 666 (2004).
- [4] Y. Zhang, Y.-W. Tan, H. L. Stormer, and P. Kim, Nature **438**, 201 (2005).
- [5] D. L. Miller, K. D. Kubista, G. M. Rutter, M. Ruan, W. A. de Heer, P. N. First, and J. A. Stroscio, Science **324**, 924 (2009).
- [6] S. Latil, V. Meunier, and L. Henrard, Phys. Rev. B **76**, 201402 (2007).
- [7] J. M. B. L. dos Santos, N. M. R. Peres, and A. H. Castro Neto, Phys. Rev. Lett. **99**, 256802 (2007).
- [8] J. Hass, F. Varchon, J. E. Millán-Otoya, M. Sprinkle, N. Sharma, W. A. de Heer, C. Berger, P. N. First, L. Magaud, and E. H. Conrad, Phys. Rev. Lett. **100**, 125504 (2008).
- [9] S. Shallcross, S. Sharma, and O. A. Pankratov, Phys. Rev. Lett. **101**, 056803 (2008).
- [10] S. Shallcross, S. Sharma, E. Kandelaki, and O. A. Pankratov, Phys. Rev. B **81**, 165105 (2010).
- [11] L. M. Guy Trambly de Laissardière, Didier Mayou, Nano Lett. **10**, 804 (2010).
- [12] E. J. Mele, Phys. Rev. B **81**, 161405 (2010).
- [13] G. Li, A. Luican, J. M. B. L. dos Santos, A. H. Castro Neto, A. Reina, J. Kong, and E. Andrei, Nature Physics **6**, 44 (2010).
- [14] R. Bistritzer and A. H. MacDonald, Phys. Rev. B **81**, 245412 (2010).
- [15] D. L. Miller, K. D. Kubista, G. M. Rutter, M. Ruan, W. A. de Heer, M. Kindermann, P. N. First, and J. A. Stroscio, Nature **6**, 811 (2010).
- [16] M. S. Dresselhaus and G. Dresselhaus, Advances in Physics **51**, 1 (2002).
- [17] A. H. Castro Neto, F. Guinea, N. M. R. Peres, K. S. Novoselov, and A. K. Geim, Rev. Mod. Phys. **81**, 109 (2009).
- [18] J. Nilsson, A. H. Castro Neto, F. Guinea, and N. M. R. Peres, Phys. Rev. B **78**, 045405 (2008).
- [19] N. B. Brandt, S. M. Chudinov, and Y. G. Ponomarev, *Semimetals I: Graphite and its Compounds* (North-Holland, Amsterdam, 1988).
- [20] D. D. L. Chung, J. Mater. Sci. **37**, 1 (2002).
- [21] W. A. de Heer, C. Berger, X. Wu, P. N. First, E. H. Conrad, X. Li, T. Li, M. Sprinkle, J. Hass, M. L. Sadowski, M. Potemski, G. Martinez, Solid State Comm. **143**, 076801 (2007).
- [22] I. Martin, Y. M. Blanter, and A. F. Morpurgo, Phys. Rev. Lett. **100**, 036804 (2008).
- [23] G. W. Semenoff, V. Semenoff, and F. Zhou, Phys. Rev. Lett. **101**, 087204 (2008).
- [24] In the generalization to multilayers the interaction between layers with  $j > 0$  needs to be added to the diagonal part  $\omega - \sum_j H_j$ .
- [25] To leading order in  $\theta$  the effect of the interlayer rotation is a space-dependent translation of the unit cells in the two layers with respect to each other. To every pair of an A-atom in the top layer and an A-atom in the bottom layer there is therefore a pair of B-atoms with the same distance and therefore the same coupling strength.
- [26] This is seen easiest when  $n + m$  is odd by the transformation  $(\chi, \chi') \rightarrow (-\chi, -\chi')$  in the expression for  $\langle \Phi_n | l(\chi, \chi') \exp(\chi^2/2 + \chi'^2/2) | \Phi_m \rangle$ .